

# Effect of $B_2O_3$ on Structure and Properties of $CaO-MgO-B_2O_3-Al_2O_3-SiO_2$ Glasses

Sanxi Huang · Sheng Li · Fengnian Wu · Yunlong Yue

Received: 7 November 2014 / Accepted: 2 January 2015 / Published online: 10 January 2015  
© Springer Science+Business Media New York 2015

**Abstract**  $xB_2O_3-(1-x)(60SiO_2-15Al_2O_3-15MgO-10CaO)$  glasses with various  $x$  around 5–30 mol% at the step of 5 mol% are prepared by the melting-quenching method at 1,450 °C for 3 h. The IR data indicate that replacing other components by  $B_2O_3$  levels up the amount of  $[BO_4]$  tetrahedron and boron-oxygen rings, forcing  $[AlO_4]$  tetrahedron to drop gradually. The glass transition temperature ( $T_g$ ), crystallization temperature ( $T_c$ ) and thermal stability ( $\Delta T$ ) rise when  $B_2O_3$  is present in lower concentrations ( $\leq 20$  mol%); accordingly the glass network enhances. However, further increase in concentration of  $B_2O_3$  ( $>20$  mol%) reduces the  $T_g$ ,  $T_c$  and  $\Delta T$ . We utilize temperature-gradient furnace to measure the G6 glass, while the re-melt sample and crystallized phase are observed from polarizing microscope destroying microstructure. As  $B_2O_3$  content move up, falls in dielectric constant ( $\epsilon_r$ ) and loss ( $\tan\delta$ ) can be associated with drop of cations polarizability as well as concentration, along with glass network rigidity ascending.

**Keywords** Aluminoborosilicate ·  $B_2O_3$  · Dielectric properties · Glass thermal stability

## 1 Introduction

Aluminoborosilicate [1, 2] glasses are widely used in composite material, flat panel display substrates and sequestration of nuclear waste, etc. Due to its excellent

dielectric properties, the non-alkali aluminoborosilicate glass fibre (E-glass fibre), is the most common reinforced materials for printed circuit board (PCB) substrate which connects different electronic devices. As the low dielectric constant is instrumental to reduce the time of signal spread and enhance characteristic impedance. Meanwhile the low dielectric loss decreases the signal attenuation. However, E-glass fibre has dielectric constant of 6.2, which has not been able to satisfy the need from high-frequency electronic field. Thus reducing dielectric constant and loss is of emergence for PCB.

$CaO-MgO-Al_2O_3-SiO_2-B_2O_3$  (CMASB) system is commonly used for E-glass. There are many literatures about structure and properties of aluminoborosilicate glasses. For example, Wu et al. indicated that higher field strength modifier cations could promote the concentration of negative charges on non-bridging oxygen, which systematically converted four-coordinated boron into three, causing changes in glass-melt properties; Darwish found that the addition of MgO at the expense of  $Al_2O_3$  dropped the fraction of  $[BO_3]$  but rose the  $[BO_4]$  groups, accompanied with the decrease of conductivity and dielectric constant. However, the dielectric loss increased; Dantas et al. pointed that with the adding/elevation of  $Fe_2O_3$ , replacing  $B_2O_3$ , the glass transition ( $T_g$ ) and crystallization ( $T_c$ ) temperature declined, which could be attributed to the drop of bond energy intensity. Also the Si–O stretching mode with one and two bridging oxygen atoms in a structural units went up, contrasting to units with three and four bridging oxygen atoms per silicon [2–4].

It is proved that  $B_2O_3$  is the network former, which can enter the glass microstructure by forming tetrahedral  $[BO_4]$  and trihedral  $[BO_3]$  in the aluminoborosilicate glass. Thus, the  $B_2O_3$  plays an important role in the structure and properties of glass. However, it is known to all that  $B_2O_3$

S. Huang · S. Li · F. Wu · Y. Yue (✉)  
Shandong Provincial Key Laboratory of Preparation and Measurement of Building Materials, School of Materials Science and Engineering, University of Jinan, Jinan 250022, China  
e-mail: yueyl@ujn.edu.cn; zztg\_yueyl@163.com

will volatilize at high temperatures, that boron-abnormal phenomenon occurs within a bounds of metal oxide content and that  $B^{3+}$  and  $Al^{3+}$  will compete to catch free oxygen, etc. The variation of  $B_2O_3$  impacts on structure and properties sophisticatedly. Accordingly, the aim of the present work is to investigate the effect of  $B_2O_3$  on structure and properties in CMASB system glass, especially the dielectric properties.

## 2 Experimental Methods

Glass samples of molar formula  $x B_2O_3-(1-x)(60SiO_2-15Al_2O_3-15MgO-10CaO)$  with  $x$  varying from 5 to 30 mol% at an interval of 5 mol% were prepared by conventional melting-quenching technique (Table 1). The accurate quantities of  $H_3BO_3$ ,  $SiO_2$ ,  $Al_2O_3$ ,  $MgO$  and  $CaO$  chemicals with high purity (>99.99 %) were weighed and mixed thoroughly, after which batches were melted in an alumina crucible at 1,723 K with electrical furnace for about 3 h. The melts were frequently stirring for a time to ensure homogeneity as well as reducing bubbles, and finally cast in stainless steel moulds to anneal at 1,173 K for 1 h, which were then removed to room temperature.

Different scanning calorimetry was carried out using Netzsch DSC-200 analyser to measure the glass transition temperature ( $T_g$ ) and/or crystallization temperature ( $T_c$ ). The SXT type of temperature-gradient furnace was used to determine crystallization region, accompanied by polarizing microscope to observe the crystallized phase of samples, and the Brookfield viscometer (Model DV-III+) was for viscosity at high temperature. Infrared spectra (IR) were measured in the range  $400-2,000\text{ cm}^{-1}$  by potassium bromide (KBr) pellet method using a Perkin-Elmer 577 infrared spectrophotometer. Before dielectric measurement, the glass samples were cut and optically polished, whose dimensions used for dielectric studies were about  $10 \times 5 \times 2\text{ mm}^3$ , with a thin coat of silver applied on either side of the glasses to serve as electrodes. The final samples were measured dielectric constant and loss using

**Table 1** Composition (mol%) of various oxide materials in studied glasses

Sample no.	Compositions					
	$SiO_2$	$Al_2O_3$	$MgO$	$CaO$	$B_2O_3$	The ratio $x$
GB1	57	14.25	14.25	9.5	5	5
GB2	54	13.5	13.5	9.0	10	10
GB3	51	12.75	12.75	8.5	15	15
GB4	48	12	12	8.0	20	20
GB5	45	11.25	11.25	7.5	25	25
GB6	42	10.5	10.5	6.0	30	30

LCR Meter (HP4294A) in the frequency range within  $10^2$  and  $10^6$  Hz.

## 3 Result and Discussion

The infrared absorption spectra of the  $B_2O_3-SiO_2-Al_2O_3-MgO-CaO$  glasses are shown in Fig. 1. We utilize the middle infrared region ( $400-2,000\text{ cm}^{-1}$ ) where the vibration modes of aluminoborosilicate glasses are active. Tables 2 and 3 summarize the major absorption band from the spectra of the investigated glasses and the vibration type of the  $B_2O_3-SiO_2-Al_2O_3$  glasses, respectively.

The IR spectra [5–7] of the glass samples show seven main absorption bands. The first band locates at  $460-480\text{ cm}^{-1}$ , which also appears in the spectra of  $B_2O_3-SiO_2$ ,  $Na_2O-B_2O_3-SiO_2$  glasses, being assumed to consist of overlapping contributions of Si–O–Si bending vibration and Si–O–Al asymmetric bending modes. Since this band is so complex and the error of experimental apparatus is large that it is hard to analyse the change of the studied glasses.

By inspection [8, 9], with the increase of  $x$ , an increasing trend displays both in the strength and frequency of the broad band at about  $640-690\text{ cm}^{-1}$ , which is supposed to the bending vibration of B–O–B in  $[BO_3]$  triangles. However, the band of stretching vibration around  $1,400\text{ cm}^{-1}$ , whose strength decreases, shows opposite results. This may be attributed to the decreasing of  $Al_2O_3$ , resulting in a decrease of  $[AlO_4]$  units. It may weaken the density of electron cloud around oxygen in  $[BO_3]$  units. Thus the decrease results in the shift between the stretching vibration and bending vibration of B–O–B in  $[BO_3]$ .

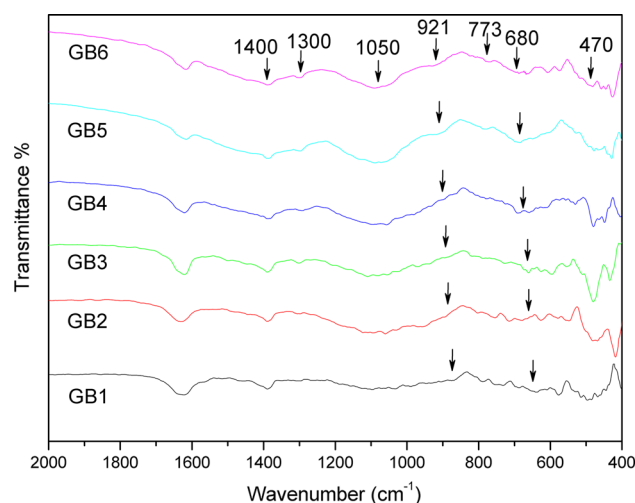


**Fig. 1** IR spectra for  $x B_2O_3-(1-x)(60SiO_2-15Al_2O_3-15MgO-10CaO)$  glasses with  $x = 5-30$  mol%

The main intense band at 860–1,100  $\text{cm}^{-1}$  belongs to a superposition of two adjacent bands—the stretching vibration of B–O–B in  $[\text{BO}_4]$  around 900  $\text{cm}^{-1}$  and the stretching vibration of Si–O–B bond, which connects  $[\text{SiO}_4]$  and  $[\text{BO}_4]$  tetrahedral structural units, around 1,050  $\text{cm}^{-1}$ , respectively. Figure 1 shows that the frequency and intensity of the 900  $\text{cm}^{-1}$  wave shift to higher value with the increase of  $\text{B}_2\text{O}_3$  while the band around 1,050  $\text{cm}^{-1}$  strengthens and narrows. That may be ascribed to the increase of  $\text{B}_2\text{O}_3$  content, enriching the  $[\text{BO}_4]$  tetrahedron. The  $[\text{BO}_4]$  and  $[\text{AlO}_4]$  units are at the network forming positions and can enter the glasses network by cross-linking with  $[\text{SiO}_4]$  or  $[\text{BO}_3]$  to form three-dimensional framework. Hence there are much more  $[\text{BO}_4]$  tetrahedron cross-linking  $[\text{SiO}_4]$  in the network, with the increase of  $\text{B}_2\text{O}_3$  while it depletes  $\text{Al}_2\text{O}_3$  [6, 10–12].

Besides, a small shoulder locates around 780  $\text{cm}^{-1}$ , where represents the bending vibration of Al–O–Al in  $[\text{AlO}_4]$ . By inspection, it is also observed that the faint absorption band of  $[\text{AlO}_4]$  is so weak that it is hard to identify the IR absorption peak, while the trend of its intensity decreases with the increase of  $x$ . On one hand, the decrease in  $\text{Al}_2\text{O}_3$  reduces concentration of  $[\text{AlO}_4]$  tetrahedron and formation of the bridging bond of Al–O–B with  $[\text{BO}_3]$ . On the other hand, it is much easier for  $\text{Al}_2\text{O}_3$  than  $\text{B}_2\text{O}_3$  to get free oxygen to form tetrahedron [13, 14]. However, the advantage of  $\text{B}_2\text{O}_3$  enhances with the increasing concentration, which leads more  $[\text{BO}_3]$  to shift to  $[\text{BO}_4]$ . As the band intensity around the 1,290  $\text{cm}^{-1}$

enhances, this shoulder band is defined as the vibration of the boroxol rings, which is composited of  $[\text{BO}_3]$  triangles and  $[\text{BO}_4]$  tetrahedrons, connected by the bridge oxygen in the glasses. Therefore, with more  $[\text{BO}_4]$  units forming, it can be realized that the formation ability of the boroxol rings improves. The result is completely in agreement with the discussion above.

In consideration of the above analysis, we can reach a conclusion that the increase of the  $\text{B}_2\text{O}_3$  improves the formation in boroxol rings and the transformation from  $[\text{BO}_3]$  triangles to  $[\text{BO}_4]$  tetrahedrons. However, the decrease in  $[\text{AlO}_4]$  and  $[\text{SiO}_4]$  units are associated with the increase in  $[\text{BO}_4]$  units. Consequently, it is difficult to identify the variation for the glass network rigidity.

Glass transition temperature ( $T_g$ ) and crystallization temperature ( $T_c$ ) are both very essential parameters for glass state characterization. In glass fibre manufacturing procedure, people think much more highly of the glass stability during wire-drawing. A common parameter [15–17] introduced by Hruby came out with the glass forming ability shown in Eq. (1), which was defined as the relation:

$$K_{\text{gl}} = \frac{T_c - T_g}{T_m - T_c} \quad (1)$$

In Eq. (1),  $K_{\text{gl}}$  and  $T_m$  are the glass forming ability and glass melting temperature, respectively. While a common and convenient parameter is the thermal stability, which is defined as  $\Delta T = T_c - T_g$ . Research in some glasses shows that higher  $\Delta T$  indicates that it is more difficult for crystallization and higher stability during formation. Figure 2 shows the differential scanning calorimetry patterns of studied glasses between 50 and 1,200  $^\circ\text{C}$ , while  $T_g$ ,  $T_c$  and  $\Delta T$  are all listed in Table 4. The majority points of  $T_g$  distribute between 930 and 960  $^\circ\text{C}$ . When  $\text{B}_2\text{O}_3$  goes up to 20 mol%,  $T_g$  improves from 935 to 959  $^\circ\text{C}$  gradually. Consequently, glass network polymerization enhances. Because the aluminoborosilicate glass network rigidity is related to the density covalent cross-link, the bridge oxygen density of the network, and the number and strength of coordinate links formed between oxygen atoms and cation. Higher values of these factors correspond to higher  $T_g$ . As a matter of fact,  $\text{B}_2\text{O}_3$  is used to be flux, which can reduce

**Table 2** The IR absorption bands observed in  $\text{Al}_2\text{O}_3$ – $\text{B}_2\text{O}_3$ – $\text{SiO}_2$  glasses

Sample no.	IR absorption band ( $\text{cm}^{-1}$ )						
GB1	1,397	1,291	1,043	865	782	642	462
GB2	1,396	1,297	1,046	877	790	659	470
GB3	1,398	1,299	1,050	892	786	665	474
GB4	1,392	1,292	1,057	900	784	672	478
GB5	1,393	1,290	1,048	910	786	684	470
GB6	1,390	1,297	1,061	921	773	680	471

**Table 3** Vibration types of the main absorption bands ( $\text{cm}^{-1}$ ) in glass samples

Absorption bands ( $\text{cm}^{-1}$ )	Vibration types
460–480	Bending vibration of Si–O–Si and Si–O–Al asymmetric bending
640–690	Bending vibration of B–O–B in $[\text{BO}_3]$ triangles
770–825	Bending vibration of Al–O in $[\text{AlO}_4]$ tetrahedron
860–925	Stretching vibration of B–O in $[\text{BO}_4]$ tetrahedron
1,030–1,080	Stretching vibration of Si–O–B in $[\text{SiO}_4]$ and $[\text{BO}_4]$ tetrahedron
1,290	Stretching vibration of boroxol rings
1,400	Stretching vibration of B–O–B in $[\text{BO}_3]$

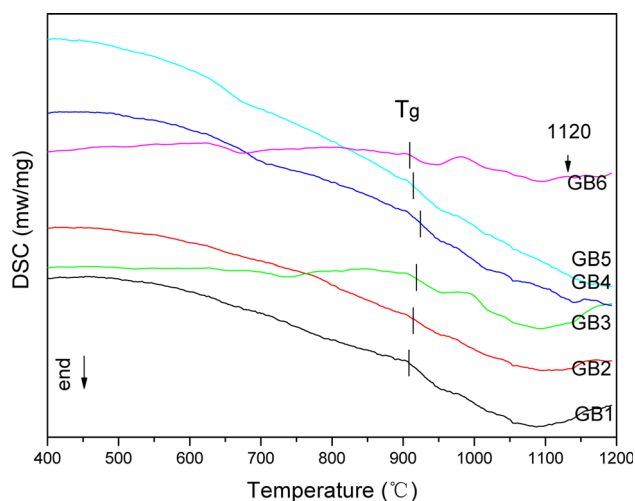


**Fig. 2** DSC curves of studied glasses at a heating rate of 10 k/min

**Table 4** Thermal characteristics as a function of the  $B_2O_3$  content

Sample no.	$T_g$ (K)	$T_c$ (K)	$\Delta T$ (K)
GB1	1,208.7	1,493.3	284.6
GB2	1,216.5	1,504.2	287.7
GB3	1,225.8	1,511.8	286
GB4	1,231.0	1,525.2	294.2
GB5	1,214.8	1,501.7	286.9
GB6	1,206.1	1,496.4	290.3

the glass viscosity and  $T_m$  by forming  $[BO_3]$  triangles at high temperature. However, during low temperature, a large number of  $[BO_3]$  triangles shift to  $[BO_4]$  tetrahedrons. The bond energy of  $[BO_4]$  units is stronger than the other glass formers. Thus, the viscosity and  $T_g$  of glasses increase. In view of IR spectra investigation, it is indicated that while the addition of  $B_2O_3$  depletes other components, a large number of  $[BO_4]$  units enter the tri-axial framework with bridge oxygen connecting with  $[SiO_4]$  and/or  $[BO_3]$  units, which improves the network rigidity and consequently increases  $T_g$  [2, 4, 18, 19].

However, further addition of  $B_2O_3$  (>20 mol%) results in decreasing of  $T_g$ , which conflicts with the aforementioned verdict of the infrared spectra examination. It can be understood that the  $[AlO_4]$  and  $[SiO_4]$  units are the main glass formers in our studied glasses. The density of covalent cross-link and the number of tetrahedrons have an important influence on  $T_g$ . The vast amount of  $[AlO_4]$  and  $[SiO_4]$  units reduce, with the expense of  $CaO$ – $MgO$ – $Al_2O_3$ – $SiO_2$ , which have damaged the microstructure strengthened by  $[BO_4]$  tetrahedrons. Moreover, alkaline earth oxygen (MO =  $MgO$  or  $CaO$ ) play a significant role in strengthening the network by providing free oxygen to

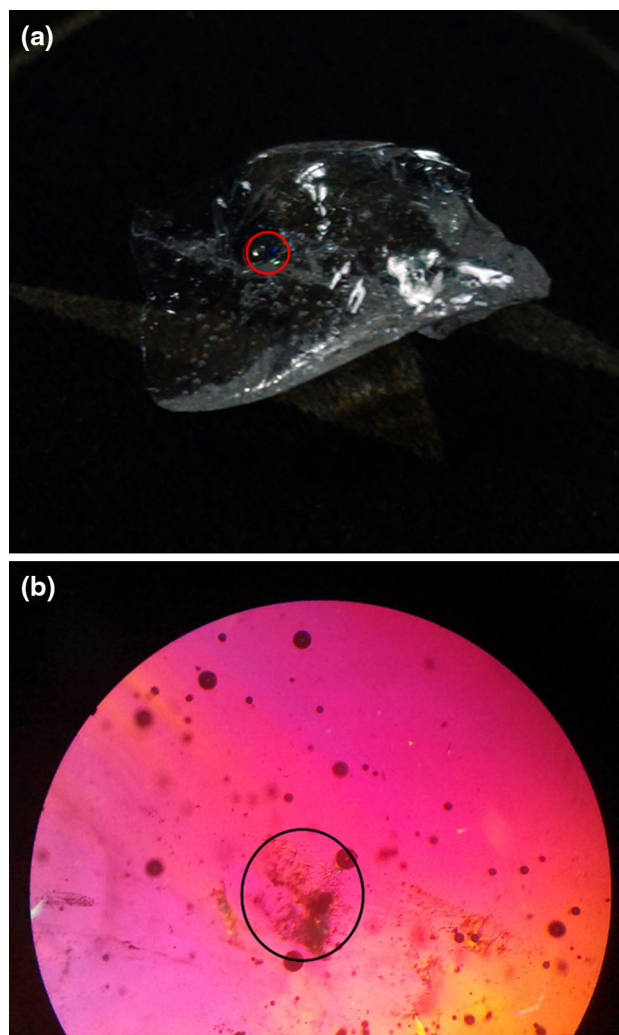


**Fig. 3** a GB6 sample after re-melted around 1,120 °C and b the morphology of polarizing microscope

shift  $[BO_3]$  to  $[BO_4]$  units. The concentration of MO bottoms out, leading to the free oxygen in the glass network decrease and accordingly prohibits  $[BO_3]$  from shifting to  $[BO_4]$  units. Even though the number of  $[BO_4]$  units increases by IR spectra measured, the  $[BO_3]$  units increase more largely than the  $[BO_4]$  in concentration, consequently leads to the glass network weaken and  $T_g$  decrease.

In view of the above-mentioned facts, it comes to the conclusion that the  $x$ , varying from 5 to 20 mol% at an interval of 5 mol%, contributes to enhancement in glass network rigidity, while the further increase will break the microstructure in glass.

From the DSC patterns, every curve shows a very weak endothermic peak, whereas the exothermic peaks due to the glass crystallization are scarcely observed. We utilize temperature-gradient furnace to measure the G6 glassed. Figure 3a, b show the re-melt sample and crystallized phase observed from polarizing microscope around



1,120 °C respectively, so do the Fig. 4a, b (around 1,300 °C). From the Fig. 3, it is found that there are only a few diopside crystals around 1,120 °C, where a shoulder exothermic peak appears in the DSC curves of GB6. However, there are so many crystallographic groups including diopside and wollastonite behind 1,300 °C that we cannot observe conspicuous endothermic peak from DSC patterns.

Thus we use the Brookfield viscometer (Model DV-III+) to measure the high temperature viscosity ( $\eta$ ), which is close related to  $T_g$  and  $T_c$ . In all viscosity equations, the temperature corresponding with the  $\eta = 10^{13}$  dpa s is the  $T_g$ , while  $T_c$ , the  $\eta = 10^{11}$  dpa s [20, 21]. Accordingly the  $T_c$  obtained from viscosity data are listed in Table 4. To compare the  $\Delta T$ , it can be observed that the increase of

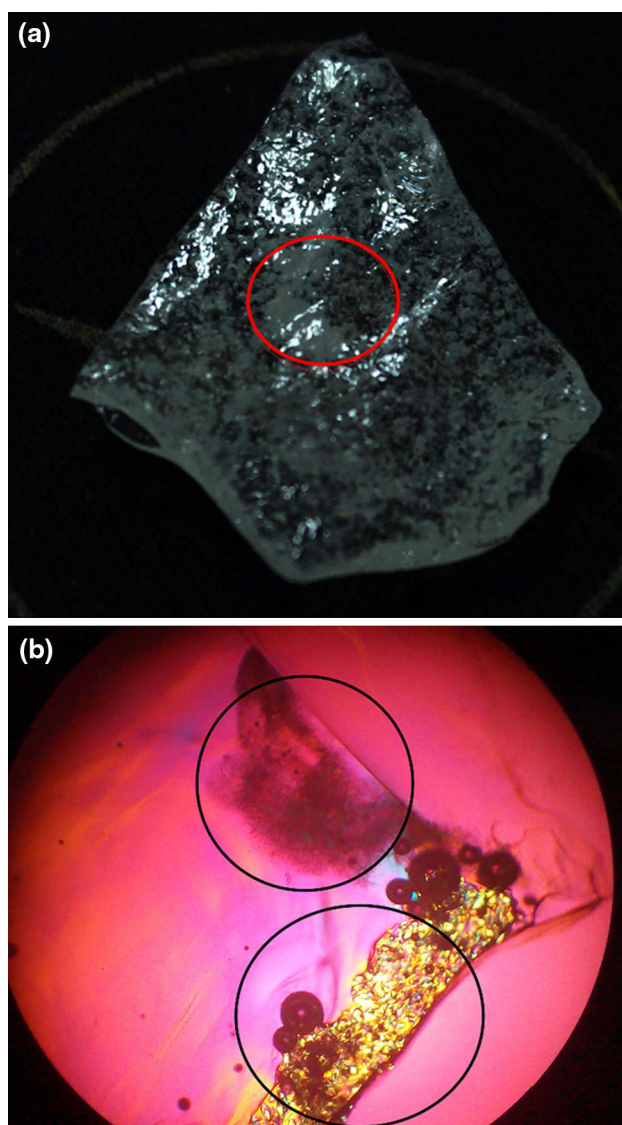


**Fig. 4** **a** GB6 sample after re-melted around 1,300 °C and **b** the morphology of polarizing microscope

$B_2O_3$ , which replaces other constituents,  $\Delta T$  increases gradually and then decreases. When the  $B_2O_3$  increases to 20 mol%,  $\Delta T$  reaches its biggest value, thus the glass thermal stability of GB4 is the best.

In our study, the dielectric properties of glass samples compose that the dielectric constant ( $\epsilon_r$ ) varies according to the frequency and  $x$  for  $x B_2O_3-(1-x)$  ( $60SiO_2-15Al_2O_3-15MgO-10CaO$ ), as well as dielectric loss ( $\tan\delta$ ). The dielectric constant of the studied glasses generates from electronic, ionic and dipole orientation mobility contributing to the polarizability. Since the frequency-dependent dielectric constant for the all studied samples is similar, there is only the sample GB1 including the 5 mol%  $B_2O_3$  within the frequency range of  $10^2-10^6$  Hz, which is plotted in the Fig. 5, exhibiting that  $\epsilon_r$  trends to decrease gradually with the rising frequency. This rule is attributed to the increase in polarizability, resulting from the ionic orientation mobility in glasses system. At low-frequency, the ionic shuttlecock (or alternating motion) period becomes large and comparable with the frequency of alternating electric field, which leads to polarizability and dielectric constant increasing consequently. However, with the frequency increasing, the ionic shuttlecock is not able to move sufficiently and rapidly any longer. As a result, the ionic oscillation will lay behind the field changes, finally resulting in the dielectric constant decreasing [22–24].

The Fig. 6 shows the variation of dielectric constant according to the content of the  $B_2O_3$  measured at 1 MHz. The increase of  $B_2O_3$  gives a decrease in the dielectric constant. Having summarized a large number of studies reached three conclusions. Firstly, there are different polarizability ( $\alpha_1$ ) [25, 26] in various cations shown in Table 5, which result in disparate impact on dielectric constant. Meanwhile, lower polarizability leads to lower dielectric constant. It is obtained that the polarizability of  $B^{3+}$  is the lowest from Table 5. Accordingly, with the

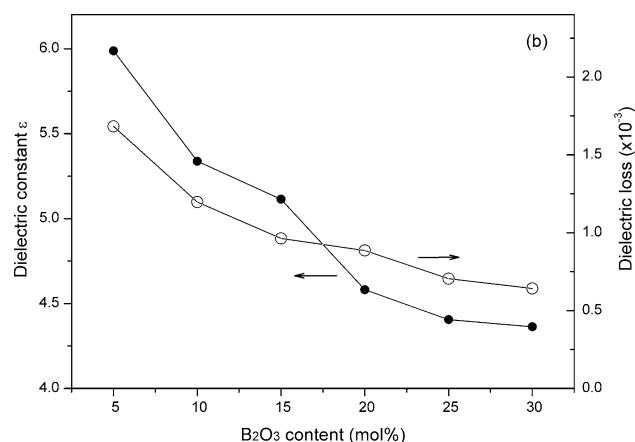


**Fig. 5** Variation of dielectric properties as a function of the frequency between  $10^2$  and  $10^6$  Hz

addition of B<sub>2</sub>O<sub>3</sub>, the dielectric constant decreased gradually. Secondly, what can be obtained is that the movement of modifying cations around the glass network interstices in the alternating electric field has a negative influence on dielectric constant [27–32]. Therefore, falls in M<sup>2+</sup> reduce the dielectric constant strongly. Besides, the mobility of modifying cations may be impacted by the densification of glass network. Higher polymerization degree with smaller structure interstices restrains migration for cations, consequently, giving rise to lower dielectric constant. While lower degree of polymerization can form a path way which can keep modifying cations moving at will. From the discussion DSC above, we may obtain that introducing B<sub>2</sub>O<sub>3</sub> up to 20 mol% strengthens the densification of glass network, while the glass network rigidity reduces as concentration is beyond 20 mol%. Thus the dielectric constant of the studied glasses should be firstly decrease and then

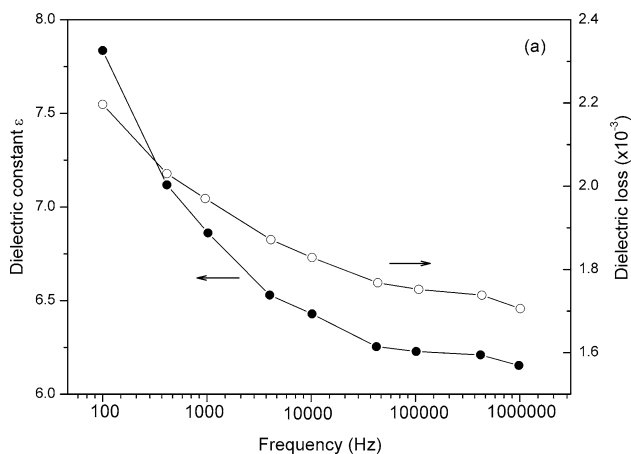


**Fig. 6** Variation of dielectric properties as a function of B<sub>2</sub>O<sub>3</sub> at 1 MHz

**Table 5** The polarizability ( $\alpha_1$ ) of different cations in glasses

Cation	$\alpha_1$	Cation	$\alpha_1$	Cation	$\alpha_1$
Si <sup>4+</sup>	0.033	Li <sup>+</sup>	0.024	Ba <sup>2+</sup>	1.595
Al <sup>3+</sup>	0.054	Na <sup>+</sup>	0.181	Pb <sup>2+</sup>	3.623
B <sup>3+</sup>	0.002	Mg <sup>2+</sup>	0.094	Ti <sup>4+</sup>	0.184
P <sup>5+</sup>	0.021	Ca <sup>2+</sup>	0.469	Y <sup>3+</sup>	0.544
Be <sup>2+</sup>	0.007	Zn <sup>2+</sup>	0.283	Ce <sup>4+</sup>	0.702

**Table 6** Dielectric properties of the glass dielectric materials in common use

Dielectric properties	The dielectric glass materials			
	E-glass	D-glass	NE-glass	Our glass (G4 sample)
Dielectric constant (at 1 MHz)	6.3	4.1	5.3	4.4
Dielectric loss (at 1 MHz)	$1.2 \times 10^{-3}$	$0.8 \times 10^{-3}$	$1.6 \times 10^{-3}$	$0.9 \times 10^{-3}$

increase. However, as is shown in Fig. 6 it can be observed that the trend of variation for dielectric constant decreases gradually with more and more B<sub>2</sub>O<sub>3</sub>. As the B<sub>2</sub>O<sub>3</sub> is beyond 20 mol%, the slope of dielectric constant curve tend to be 0. We can assume that it is the polarizability of B<sup>3+</sup> that plays a leading role in dielectric constant, when compares with the polymerization.

The dielectric loss of the studied glasses generate from ion migration losses, ion vibration losses as well as electron polarization losses [33, 34]. It can be found that the variation of dielectric loss about GB1 sample is similar with dielectric constant from Fig. 5—with the increase in frequency, dielectric loss decreases. This behaviour relies on the influence of electric field, which enhances the electron polarization by assisting electron hopping between two sites. At lower frequency, the charge carriers can hop easily with lower free energy between two sites and tend to gather at the sites with higher free-energy barriers, which results in a network electron polarization and consequently gives an increase in dielectric loss. While at higher frequency, the alternating period of the electric field is so rapid that the charge carriers cannot be able to hop sufficiently and the polarization due to the charges accumulating at higher free-energy barrier sites reduced, which leads to an decrease in the dielectric loss [35]. Moreover, the movement of modifying cations has an important role in dielectric loss. The alkaline-earth metal cations can pass through the glass network easily under the applied electric field with lower frequency and then forms conductivity loss, which leads to a decrease of dielectric loss. However, the metal cations cannot be able to migrate rapidly any longer, which is owing to their movement beginning to lay behind the alternating electric field when the frequency increases, resulting in an increase of dielectric loss. Meanwhile, Fig. 6 represents that dielectric loss decreases consistently with the B<sub>2</sub>O<sub>3</sub> increase at 1 MHz. It may be attributed to that MO declining gives rise to decrease in the concentration of charge cations so that fewer cations, participating in the migration and polarization, reduced, resulting in a decrease of dielectric loss [36, 37].

In our study, the G4 sample is the best with dielectric constant of 4.4 and dielectric loss of 0.0009 in consideration of the volatilization of boron and cost of production. Compared with other dielectric materials used in common shown in Table 6, D-glass is the best dielectric material. However, it is hard to produce in general technology,

which is due to the melting temperature and production cost of D-glass are much larger than those of others. In our study, the G4 glass material, manufactured in common technology and facilities, has better dielectric properties than the E-glass and T-glass, which means better commercial value [15, 38].

#### 4 Conclusions

It has been observed that the addition of  $B_2O_3$  on structure and physical properties of  $xB_2O_3-(1-x)(60SiO_2-15Al_2O_3-15MgO-10CaO)$  ( $x = 5, 10, 15, 20, 25$  and  $30$  mol%) glasses is investigated. IR result indicates that  $B_2O_3$  acts as network former and more  $[BO_4]$  units replace  $[AlO_4]$  tetrahedrons, which causes network tightening. This can also be proved by the DSC data. When  $B_2O_3$  reaches up to 20 mol%,  $T_g$ ,  $T_c$  and  $\Delta T$  continue to increase and then decrease with further addition of  $B_2O_3$ . It is indicated that the glass network rigidity and the thermal stability are the best at the 20 mol%. The parameters  $\epsilon_r$  and  $\tan\delta$  come to reduce with an increase of the frequency as well as  $B_2O_3$ . This behaviour can be attributed to the tightening network and polarization owing to charge cations varying.

**Acknowledgments** This work is supported by Natural Science Foundation of Shandong Province (Nos. ZR2012EMM019), Natural Science Foundation of Shandong Province (Nos. ZR2011EMQ005) and Natural Science Foundation (Nos. 51172093, 51042009).

#### References

- X. Zhang, Y. Yue, H. Wu, J. Mater. Sci. **24**, 8 (2013)
- A. Dahshan, J. Non-Cryst. Solids **354**, 26 (2008)
- J. Wu, J.F. Stebbins, J. Non-Cryst. Solids. **362**, (2013)
- N.O. Dantas, W.E. Ayta, A.C. Silva, N.F. Cano, S.W. Silva, P.C. Morais, Spectrochim Acta. A **81**, 1 (2011)
- A. Efimov, J. Non-Cryst. Solids. **203**, (1996)
- Y. Cheng, H. Xiao, W. Guo, W. Guo, Ceram. Int. **33**, 7 (2007)
- H. Darwish, M. Gomaa, J. Mater. Sci. **17**, 1 (2006)
- Y. Cheng, H. Xiao, C. Shuguang, B. Tang, Phys. B **404**, 8–11 (2009)
- T. Sun, H. Xiao, W. Guo, X. Hong, Ceram. Int. **36**, 2 (2010)
- M. Arora, S. Baccaro, G. Sharma, D. Singh, K.S. Thind, D.P. Singh, Nucl. Instrum. Meth. B **267**, 5 (2009)
- G. El-Damrawi, K. El-Egili, Phys. B **299**, 1 (2001)
- E. Kamitsos, A. Patsis, G.D. Chryssikos, J. Non-Cryst. Solids **152**, 2 (1993)
- L.-S. Du, J.F. Stebbins, J. Non-Cryst. **351**, 43–45 (2005)
- V. Gerasimov, O. Spirina, Glass Ceram. **61**, 5–6 (2004)
- M. Reben, H. Li, Int. J. Appl. Glass Sci. **2**, 2 (2011)
- A. Hrubý, Czech. J. Phys. B **22**, 11 (1972)
- S. Mahadevan, A. Giridhar, A. Singh, J. Non-Cryst. Solids **88**, 1 (1986)
- A.S. Weber, R. Hodyss, P.V. Johnson, K. Willacy, I. Kanik, Astrophys. J. **703**, 1 (2009)
- P.A. Bingham, R.J. Hand, S.D. Forder, Mater. Res. Bull. **41**, 9 (2006)
- K. Joseph, K.V.G. Kutty, M.C. Goswami, P.R.V. Rao, Thermochim. Acta **587**, (2014)
- J. Chovanec, M. Chromčíková, P. Pilný, J. Šánělová, J. Málek, M. Liška, J. Therm. Anal. Calorim. **114**, 3 (2013)
- X. Zhang, Z. Du, H. Wu, Y. Yue, Surf. Rev. Lett. **20**, 03 (2013)
- S.-P. Szu, C.-Y. Lin, Mater. Chem. Phys. **82**, 2 (2003)
- S. Sindhu, S. Sanghi, A. Agarwal, V. Seth, N. Kishore, Mater. Chem. Phys. **90**, 1 (2005)
- V. Dimitrov, T. Komatsu, J. Solid State Chem. **163**, 1 (2002)
- T. Inoue, T. Honma, V. Dimitrov, T. Komatsu, J. Solid State Chem. **183**, 12 (2010)
- B.H. Jung, D.N. Kim, H.-S. Kim, J. Non-Cryst. Solids **351**, 40 (2005)
- Y. Yue, X. Zhang, Y. Xu, S. Huang, P. Chen, Mater. Lett. (2014)
- M. Gomaa, H. Abo-Mosallam, H. Darwish, J. Mater. Sci. **20**, 6 (2009)
- G. Srinivasarao, N. Veeraiiah, J. Solid State Chem. **166**, 1 (2002)
- G. Srinivasarao, N. Veeraiiah, J. Phys. Chem. Solids **63**, 4 (2002)
- B.-H. Jung, S.-J. Hwang, H.-S. Kim, J. Eur. Ceram. Soc. **25**, 13 (2005)
- J. Lumeau, L. Glebova, G.P. Souza, E.D. Zanotto, L.B. Glebov, J. Non-Cryst. Solids **354**, 42 (2008)
- T. Zhang, M.-Q. Wu, S.-R. Zhang, J. Xiong, J.-M. Wang, D.-H. Zhang, F.-M. He, Z.-P. Li, Chin. Phys. B **21**, 7 (2012)
- S. Ramesh, A. Yahaya, A. Arof, Solid State Ionics **152**, (2002)
- R.S. Gedam, D.D. Ramteke, J. Phys. Chem. Solids **74**, 7 (2013)
- F. Salman, A. Mekki, J. Non-Cryst. Solids **357**, 14 (2011)
- E. Ozel, H. Yurdakul, S. Turan, M. Ardit, G. Cruciani, M. Dondi, J. Eur. Ceram. Soc. **30**, 16 (2010)